Unconventional scanning tunneling conductance spectra for graphene

K. Saha,[1] I. Paul,[2,3] and K. Sengupta[1]
[1]*Theoretical Physics Division, Indian Association for the Cultivation of Sciences, Kolkata 700032, India*
[2]*Institut Néel, CNRS/UJF, 25 Avenue des Martyrs, BP 166, 38042 Grenoble, France*
[3]*Institut Laue-Langevin, 6 rue Jules Horowitz, BP 156, 38042 Grenoble, France*
(Received 16 June 2009; revised manuscript received 8 February 2010; published 30 April 2010)

We compute the tunneling conductance of graphene as measured by a scanning tunneling microscope (STM) with a normal/superconducting tip. We demonstrate that for undoped graphene with zero Fermi energy, the *first derivative* of the tunneling conductance with respect to the applied voltage is proportional to the density of states of the STM tip. We also show that the shape of the STM spectra for graphene doped with impurities depends qualitatively on the position of the impurity atom in the graphene matrix and relate this unconventional phenomenon to the pseudospin symmetry of the Dirac quasiparticles in graphene. We suggest experiments to test our theory.

DOI: 10.1103/PhysRevB.81.165446 PACS number(s): 81.05.U−, 07.79.Cz, 73.20.Hb, 73.40.Gk

I. INTRODUCTION

The low-energy quasiparticles of graphene around K and K' Fermi points have Dirac-type properties.[1] In particular, the pseudospin of these quasiparticles around $K(K')$ points along (opposite to) their direction of motion. The presence of such Dirac-type quasiparticles with definite helicity leads to a number of unusual electronic properties in graphene.[2–5] Recently, the influence of such Dirac quasiparticles on properties of graphene doped with magnetic/nonmagnetic impurities have attracted theoretical and experimental attention.[6–11] However, the recent experimental observation of dependence of STM tunneling spectra on the position of the impurity in the graphene matrix in Ref. 9 lacks a theoretical explanation even at a qualitative level.[10]

Scanning tunneling microscopes (STM) are extremely useful probes for studying properties of two or quasi-two-dimensional materials.[11,12] Studying electronic properties of a sample with STM typically involves measurement of the tunneling conductance $G(V)$ for a given applied voltage V. The tunneling conductances measured in these experiments have also been studied theoretically for conventional metallic systems and are known to exhibit Fano resonances at zero-bias voltage in the presence of impurities.[13,14] The application and utility of this experimental technique, with superconducting STM tips, have also been discussed in the literature for conventional systems.[15] However, tunneling spectroscopy of graphene using superconducting STM tips remains to be studied both experimentally and theoretically.

In this work, we compute the STM response of doped graphene and demonstrate that the STM spectra has several unconventional features. For undoped graphene with Fermi energy $E_F=0$, the derivative of the STM tunneling conductance (G) with respect to the applied voltage (dG/dV) reflects the density of states (DOS) of the STM tip (ρ_t), i.e., $dG/dV \sim +(-)\rho_t$ for $V>(<)0$. By tuning E_F, one can interpolate between this unconventional $\rho_t \sim \pm dG/dV$ and the conventional $\rho_t \sim G$ (seen for $E_F \gg eV$) behaviors. Further, we find that for superconducting STM tips with energy gap Δ_0, $G(dG/dV)$ displays a cusp (discontinuity) at $eV=-E_F-\Delta_0$ as a signature of the Dirac point which should be experimentally observable in graphene with small E_F where the regime $eV>E_F$ can be easily accessed. For impurity-doped graphene with large E_F, experiments in Ref. 9 have seen that the tunneling conductance, as measured by a metallic STM tip, depends qualitatively on the position of the impurity in the graphene matrix. For impurity atoms atop the hexagon center, the zero-bias tunneling conductance shows a peak; for those atop a graphene site, it shows a dip. We provide a qualitative theoretical explanation of this phenomenon and show that this unconventional behavior is a consequence of conservation/breaking of pseudospin symmetry of the Dirac quasiparticles by the impurity. We also predict that tuning E_F to zero by a gate voltage would not lead to qualitative change in shape of the conductance spectra when the impurity is atop the hexagon center; for impurity atop a site, the tunneling conductance would change from a dip to a peak via an antiresonance.

The organization of the rest of the paper is as follows. In Sec. II, we present the derivation of the tunneling current. This is followed by Sec. III where we present our main results. Finally we conclude in Sec. IV.

II. COMPUTATION OF TUNNELING CURRENT

The experimental situation for STM measurement is schematically represented in Fig. 1. The STM tip is placed atop the impurity and the tunneling current $\mathcal{I}$ is measured as a function of applied bias voltage V. The possible positions of the impurity is shown in the right panel of Fig. 1. Such a situation can be modeled by the well-known Anderson Hamiltonian.[16] Here we incorporate the low-energy Dirac quasiparticles of graphene in this Hamiltonian which is given by

$$H = H_G + H_d + H_t + H_{Gd} + H_{Gt} + H_{dt}, \tag{1}$$

$$H_G = \int_k \psi_s^{\beta\dagger}(\vec{k})[\hbar v_F(\tau_z\sigma_x k_x + \sigma_y k_y) - E_F I]\psi_s^{\beta}(\vec{k}), \tag{2}$$

$$H_d = \sum_{s=\uparrow,\downarrow} \epsilon_d d_s^\dagger d_s + U n_\uparrow n_\downarrow, \tag{3}$$

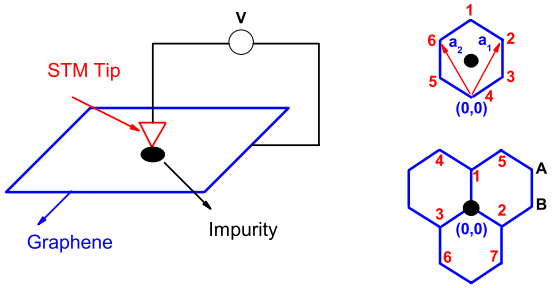

FIG. 1. (Color online) Schematic experimental setup with the right panel showing two possible positions (atop hexagon center and atop a B site) of the impurity. The numbers denote nearest-neighbor A and B sublattice sites to the impurity. $a_{1(2)}=+(-)\sqrt{3}/2\hat{x}+3/2\hat{y}$ [lattice spacing set to unity] are graphene lattice vectors. The choice of coordinate center (0,0) are shown for each case.

$$H_t = \sum_{\nu} [\sum_{s=\uparrow\downarrow} \epsilon_{t\nu} \tilde{t}^{\dagger}_{\nu s} \tilde{t}_{\nu s} + (\Delta_0 \tilde{t}^{\dagger}_{\nu\uparrow} \tilde{t}^{\dagger}_{-\nu\downarrow} + \text{H.c.})], \tag{4}$$

$$H_{Gd} = \sum_{\alpha=A,B} \int_k [V^0_{\alpha}(\vec{k}) c^{\beta}_{\alpha,s}(\vec{k}) d^{\dagger}_s + \text{H.c.}], \tag{5}$$

$$H_{dt} = \sum_{s=\uparrow,\downarrow;\nu} (W^0_{\nu} \tilde{t}_{\nu s} d^{\dagger}_s + \text{H.c.}), \tag{6}$$

$$H_{Gt} = \sum_{\alpha=A,B;\nu} \int_k [U^0_{\alpha;\nu}(\vec{k}) c^{\beta}_{\alpha,s}(\vec{k}) \tilde{t}^{\dagger}_{\nu s} + \text{H.c.}]. \tag{7}$$

Here H_G is the Dirac Hamiltonian for the graphene electrons which are described by the two-component annihilation operator

$$\psi^{\beta}_s(\vec{k}) = [c^{\beta}_{As}(\vec{k}), c^{\beta}_{Bs}(\vec{k})] \tag{8}$$

belonging to the valley $\beta=K,K'$ and spin $s=\uparrow,\downarrow$, I is the identity matrix, τ and σ denote Pauli matrices in valley and pseudospin spaces, v_F is the Fermi velocity, and $\int_k \equiv \Sigma_{\beta=K,K'} \Sigma_{s=\uparrow\downarrow} \int \frac{d^2k}{(2\pi)^2}$. H_d denotes the impurity-atom Hamiltonian with an on-site energy ϵ_d and U is the strength of on-site Hubbard interaction. H_t is the Hamiltonian for the superconducting ($\Delta_0 \neq 0$) or metallic ($\Delta_0=0$) tip electrons with on-site energy $\epsilon_{t\nu}$, where ν signifies all quantum numbers (except spin) associated with the tip electrons. The operators d_s and $\tilde{t}_{\nu s}$ are the annihilation operators for the impurity and the tip electrons. The Hamiltonians H_{Gd}, H_{Gt}, and H_{dt} describe hopping between the graphene and the impurity electrons, the graphene and the STM tip electrons, and the impurity and the STM tip electrons, respectively. The corresponding parameters $V^0_{\alpha}(\vec{k})$, $U^0_{\alpha;\nu}(\vec{k})$, and W^0_{ν} are taken to be independent of valley and spin indices of graphene electrons but may depend on their sublattice index or pseudospin. Note that the tunneling terms [Eq. (5)] automatically take into account potential scattering; such terms are generated once the impurity degree of freedom is integrated out unless there is perfect particle-hole symmetry ($E_F=0$).

The tunneling current for the present model is given by

$$\mathcal{I}(t) = e\langle dN_t/dt \rangle = ie\langle [H, N_t] \rangle/\hbar, \tag{9}$$

where $N=\Sigma_{\nu s} \tilde{t}^{\dagger}_{\nu s} \tilde{t}_{\nu s}$ is the number operator for the tip electrons. These commutators receive contribution from H_{dt} and H_{Gt} in Eqs. (6) and (7) and can be written as

$$\mathcal{I}(t) = \frac{e}{\hbar} \{ \sum_{\sigma\nu} [W^{0*}_{\nu} \mathcal{G}^{(2)<}_{\sigma\nu}(t) - W^0_{\nu} \mathcal{G}^{(2)<}_{\nu\sigma}(t)] + \int_k \sum_{\sigma\nu} [U^{0*}_{\nu}(\vec{k}) G^{(1)<}_{\sigma\nu}(t;\vec{k}) - U^0_{\nu}(\vec{k}) G^{(1)<}_{\nu\sigma}(t;\vec{k})] \}, \tag{10}$$

where we define the standard Keldysh Green's functions $\mathcal{G}$ and G as[17]

$$G^{(1)<}_{\sigma\nu}(t;\vec{k}) = -i\langle \tilde{t}^{\dagger}_{\nu\sigma}(t) \psi_{\sigma}(0;\vec{k}) \rangle,$$

$$G^{(1)<}_{\nu\sigma}(t;\vec{k}) = -i\langle \psi^{\dagger}_{\sigma}(t;\vec{k}) \tilde{t}_{\nu\sigma}(0) \rangle,$$

$$\mathcal{G}^{(2)<}_{\sigma\nu}(t) = -i\langle \tilde{t}^{\dagger}_{\nu\sigma}(t) d_{\sigma}(0) \rangle,$$

$$\mathcal{G}^{(2)<}_{\nu\sigma}(t) = -i\langle d^{\dagger}_{\sigma}(t) \tilde{t}_{\nu\sigma}(0) \rangle. \tag{11}$$

These hybrid Green's functions [Eq. (11)] obey the usual Keldysh relations. For example, $\mathcal{G}^{(2)<}_{\sigma\nu}$ and $\mathcal{G}^{(2)>}_{\sigma\nu}$ can be expressed in terms of the time ordered ($\mathcal{G}^{(2)t}_{\sigma\nu}$), antitime ordered ($\mathcal{G}^{(2)\bar{t}}_{\sigma,\nu}$), retarded ($\mathcal{G}^{(2)R}_{\sigma,\nu}$), and advanced ($\mathcal{G}^{(2)A}_{\sigma,\nu}$) Keldysh Green's functions as[17]

$$\mathcal{G}^{(2)t}_{\sigma\nu} + \mathcal{G}^{(2)\bar{t}}_{\sigma\nu} = \mathcal{G}^{(2)<}_{\sigma\nu} + \mathcal{G}^{(2)>}_{\sigma\nu},$$

$$\mathcal{G}^{(2)R}_{\sigma\nu} - \mathcal{G}^{(2)A}_{\sigma\nu} = \mathcal{G}^{(2)>}_{\sigma\nu} - \mathcal{G}^{(2)<}_{\sigma\nu}. \tag{12}$$

Similar relations hold for $G^{(1)<}_{\sigma\nu}(t;\vec{k})$ and $G^{(1)<}_{\nu\sigma}(t;\vec{k})$.

Next, we expand the hybrid Green's functions $G^{(1)<}_{\sigma\nu}(t;\vec{k})$, $G^{(1)<}_{\nu\sigma}(t;\vec{k})$, $\mathcal{G}^{(2)<}_{\sigma\nu}(t)$, and $\mathcal{G}^{(2)<}_{\nu\sigma}(t)$ in perturbation series.[17] After some straightforward algebra, one obtains, to first order in perturbation theory,

$$G^{(1)<}_{\sigma\nu}(k) = \int_{k'} \sum_{\sigma'\nu'} U^0_{\nu'}(\vec{k}') [g^{t}_{\nu'\sigma';\nu\sigma} \mathcal{G}^{<}_{\sigma,\sigma'}(\vec{k},\vec{k}') - g^{<}_{\nu'\sigma';\nu\sigma} \mathcal{G}^{\bar{t}}_{\sigma,\sigma'}(\vec{k},\vec{k}')] + \sum_{\sigma'\sigma} W^0_{\nu'} \times [g^{t}_{\nu'\sigma';\nu\sigma} G^{h<}_{\sigma\sigma'}(\vec{k}) - g^{<}_{\nu'\sigma';\nu\sigma} G^{h\bar{t}}_{\sigma\sigma'}(\vec{k})],$$

$$G^{(1)<}_{\nu\sigma}(\vec{k}) = \int_{k'} \sum_{\sigma'\nu'} U^{0*}_{\nu'}(\vec{k}') [g^{<}_{\nu\sigma;\nu'\sigma'} \mathcal{G}^{t}_{\sigma',\sigma}(\vec{k},\vec{k}') - g^{\bar{t}}_{\nu\sigma;\nu'\sigma'} \mathcal{G}^{<}_{\sigma',\sigma}(\vec{k},\vec{k}')] + \sum_{\sigma'\nu'} W^{0*}_{\nu'} \times [g^{<}_{\nu\sigma;\nu'\sigma'} G^{ht}_{\sigma'\sigma}(\vec{k}) - g^{\bar{t}}_{\nu\sigma;\nu'\sigma'} G^{h<}_{\sigma';\sigma}(\vec{k})],$$

$$\mathcal{G}^{(2)<}_{\sigma\nu} = \int_{k'} \sum_{\sigma'\nu'} U^0_{\nu}(\vec{k}')[g^t_{\nu'\sigma';\nu\sigma} G^{h<}_{\sigma\sigma'}(\vec{k}') - g^<_{\nu'\sigma';\nu\sigma} G^{(h\bar{t}}_{\sigma\sigma'}(\vec{k}')] + \sum_{\sigma'\nu'} W^0_{\nu'} \times [g^t_{\nu'\sigma';\nu\sigma} G^{d<}_{\sigma\sigma'} - g^<_{\nu'\sigma';\nu\sigma} G^{d\bar{t}}_{\sigma\sigma'}],$$

$$\mathcal{G}^{(2)<}_{\nu\sigma} = \int_{k'} \sum_{\sigma'\nu'} U^{0*}_{\nu'}(\vec{k}')[g^<_{\nu\sigma;\nu'\sigma'} G^{ht}_{\sigma',\sigma}(\vec{k}') - g^{\bar{t}}_{\nu\sigma;\nu'\sigma'} G^{h<}_{\sigma,\sigma'}(\vec{k}')] + \sum_{\sigma'\nu'} W^{0*}_{\nu'} \times [g^<_{\nu\sigma;\nu'\sigma'} G^{ht}_{\sigma'\sigma}(\vec{k}') - g^{\bar{t}}_{\nu\sigma;\nu'\sigma'} G^{h<}_{\sigma'\sigma}(\vec{k}')], \tag{13}$$

where all the Green's functions appearing in Eq. (13) are at the same time t which we have not written out explicitly for clarity. In Eq. (13), $g^<_{\nu\sigma;\nu'\sigma'}(t) = -i\langle \tilde{t}^\dagger_{\nu\sigma}(t)\tilde{t}_{\nu'\sigma'}(0)\rangle$ denotes the Green's function for the tip electrons which, in frequency space, is given by

$$g^<_{\nu\sigma;\nu'\sigma'}(\omega) = 2\pi i f(\epsilon_{t\nu} - \mu_t)\delta_{\nu\nu'}\delta_{\sigma\sigma'}\delta(\omega - \epsilon_{t\nu}), \tag{14}$$

where $f(x) = 1/(1+\exp[x/k_BT])$ denotes the Fermi-Dirac distribution function at a temperature T, μ_t is the chemical potential for the tip electrons, and k_B is the Boltzmann constant. Similar expressions can be obtained for g^t and $g^{\bar{t}}$ using Eq. (12).[17] $\mathcal{G}^<_{\sigma\sigma'}(t;\vec{k},\vec{k}') = -i\langle \psi^\dagger_{\sigma'}(t;\vec{k})\psi_\sigma(0;\vec{k}')\rangle$ denotes the Green's function of the Dirac electrons in the presence of the impurity. The retarded and advanced components of this Green's function which we shall need in subsequent analysis can be written as

$$\mathcal{G}^{R(A)}_{\sigma\sigma'}(\vec{k},\vec{k}') = \delta_{\sigma\sigma'}\delta(\vec{k}-\vec{k}')\mathcal{G}^{(0)R(A)}_{\sigma}(\vec{k}) + \int_{k_1}\int_{k_2}\sum_{\sigma_1,\sigma_2} V^{0*}(\vec{k})V^0(\vec{k}')\mathcal{G}^{R(A)}_{\sigma\sigma_1}(\vec{k},\vec{k}_1) \times G^{dR(A)}_{\sigma_1\sigma_2}(\vec{k}_1,\vec{k}_2)\mathcal{G}^{R(A)}_{\sigma_2\sigma'}(\vec{k}_2,\vec{k}'), \tag{15}$$

where again it is understood that all Green's functions are at a given time t and $G^{dR(A)}_{\sigma\sigma'}(t) = -i\langle d^\dagger_\sigma(t)d_{\sigma'}(0)\rangle$ denotes the retarded (advanced) Green's function of the interacting impurity electrons. In frequency space, this Green's function is given by

$$G^{dR(A)}_{\sigma\sigma'}(\omega) = \frac{\delta_{\sigma\sigma'}}{\omega - \epsilon_d - \mathrm{Re}[\Sigma_d(\omega)] - (+)i\,\mathrm{Im}[\Sigma_d(\omega)]}, \tag{16}$$

where $\Sigma_d(\omega)$ denotes the self-energy of the impurity in the absence of the tip. Σ_d receives contributions from both the on-site Hubbard interaction U of the impurity electrons and the coupling of the impurity to the Dirac electrons. Note that we have neglected the effect of the STM tip while computing $\mathcal{G}^{R(A)}_{\sigma\sigma'}(t;\vec{k},\vec{k}')$ which is justified as long as we restrict ourselves to linear-response theory. In Eq. (15), $\mathcal{G}^{(0)R(A)}_{\sigma}(t;\vec{k})$ denotes the single-particle Green's function for the graphene electrons in the absence of the impurity and the STM tip and is given, in frequency space, by

$$\mathcal{G}^{(0)R(A)}_{\sigma}(\omega,\vec{k}) = \frac{(\omega+E_F)I - \hbar v_F(\tau_z\sigma_x k_x + \sigma_y k_y)}{(\omega+E_F)^2 - \hbar^2 v_F^2|\vec{k}|^2 - (+)i\eta}. \tag{17}$$

Finally, the Green's function $G^{h<}_{\sigma\sigma'}(t;\vec{k}) = -i\langle d^\dagger_\sigma(t)\psi_{\sigma'}(0;\vec{k})\rangle$ used in Eq. (13) is a hybrid Green's function whose retarded and advanced components are given, within first-order perturbation theory, by

$$G^{hR(A)}_{\sigma\sigma'}(t;\vec{k}) = \sum_{\sigma_1} V^0(\vec{k})\mathcal{G}^{(0)R(A)}_{\sigma\sigma_1}(0;\vec{k})\mathcal{G}^{dR(A)}_{\sigma_1\sigma'}(t). \tag{18}$$

Next we follow Ref. 14 to substitute Eqs. (13) and (14) in Eq. (10) and approximate the coupling functions to be independent of momentum: $U^0(\vec{k}) \equiv U^0$, $W^0_\nu \equiv W^0$, and $V^0(\vec{k}) \equiv V^0$. Such an approximation is justified as long we restrict ourselves to low applied voltages. With this approximation, after some algebra involving Eqs. (10)–(18), one obtains the expression of the current

$$\mathcal{I} = \mathcal{I}_0\int_{-\infty}^{\infty} d\omega[f(\omega - eV) - f(\omega)]\rho_t(\omega - eV)\left\{\rho_G(\omega)\times|U^0|^2 + \frac{|B(\omega)|^2}{\mathrm{Im}\,\Sigma_d(\omega)}\frac{|q(\omega)|^2 - 1 + 2\,\mathrm{Re}[q(\omega)]\chi(\omega)}{[1+\chi^2(\omega)](1+\xi^2)}\right\}, \tag{19}$$

where $\mathcal{I}_0 = 2e(1+\xi^2)/h$, $\rho_G(\epsilon)$ and $\rho_t(\epsilon)$ are the graphene and STM tip electron DOS, respectively, $\xi = |U^0_B|/|U^0_A| = |V^0_B|/|V^0_A|$ is the ratio of coupling of the impurity to the electrons in B and A sites of graphene with $U^0_A = U^0$ and $V^0_A = V^0$, and $\Sigma_d(\epsilon)$ is the impurity advanced self-energy in the absence of the tip. Here $B(\epsilon) = V^0U^0I_2(\epsilon)$ and $q(\epsilon)$ and $\chi(\epsilon)$ are given by

$$q(\epsilon) = [W^0/U^0 + V^0I_1(\epsilon)]/[V^0I_2(\epsilon)],$$

$$\chi(\epsilon) = \frac{\epsilon - \epsilon_d - \mathrm{Re}\,\Sigma_d(\epsilon)}{\mathrm{Im}\,\Sigma_d(\epsilon)}, \tag{20}$$

where we have neglected the energy dependence of the coupling functions assuming small applied voltages. In Eq. (20), $I_1(\epsilon) = (1+\xi^2)\Sigma_k\mathrm{Tr}[\mathrm{Re}\{\mathcal{G}^{(0)R}_\sigma(\epsilon,\mathbf{k})\}]$, $I_2(\epsilon) = (1+\xi^2)\Sigma_k\mathrm{Tr}[\mathrm{Im}\{\mathcal{G}^{(0)R}_\sigma(\epsilon,\mathbf{k})\}]$, and Tr denotes trace over Pauli matrices in pseudospin, valley and spin spaces. Substituting Eq. (17) in Eq. (20), we find[7,14]

$$I_1(\epsilon) = -4(1+\xi^2)(\epsilon+E_F)\ln|1 - \Lambda^2/(\epsilon+E_F)^2|/\Lambda^2,$$

$$I_2(\epsilon) = 4(1+\xi^2)\pi|\epsilon+E_F|\theta(\Lambda - \epsilon - E_F)/\Lambda^2, \tag{21}$$

where Λ is the ultraviolet momentum cutoff and θ is the Heaviside step function. Usually, in graphene, Λ is taken to be the energy at which the graphene bands start bending rendering the low-energy Dirac theory inapplicable and can be estimated to be 1–2 eV.[6]

Equations (19)–(21) constitute the central results of this section and yields the tunneling current through the STM tip within linear-response theory. We are going to analyze these equations in the subsequent sections.

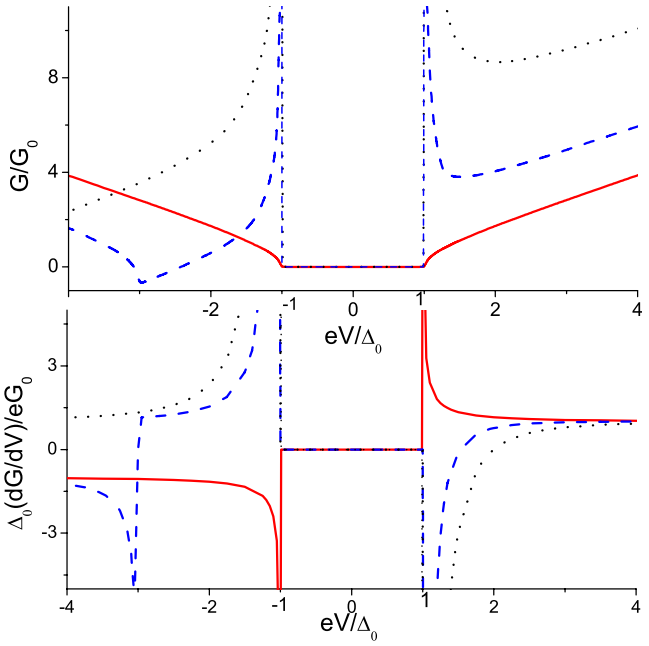

FIG. 2. (Color online) Plot of the tunneling conductance G and its derivative dG/dV as a function of the applied bias voltage $eV/\Delta_0=-p$ for $r=0,2,6$ (red solid, blue dashed, and black dotted lines), respectively. See text for details.

III. RESULTS

In this section, we are going to analyze the tunneling conductance $[G(V)=d\mathcal{I}/dV]$ as measured by the STM tip. First we consider the case of a superconducting tip in the absence of any impurity. In this case, the contribution to the conductance comes from the first term of Eq. (19). For s-wave superconducting tips, one finds that the tunneling conductance $[G(V)=d\mathcal{I}/dV]$ for $E_F>0$ and at $T=0$ is given by (with $r=E_F/\Delta_0$, $p=-eV/\Delta_0$)

$$G = G_0[\mathcal{N}_t(p)|r| + \int_p \mathrm{sgn}(z-p+r)\mathcal{N}_t(z)dz], \tag{22}$$

$$\frac{dG}{dV} = \frac{eG_0}{\Delta_0}[\mathcal{N}_t(p) - \mathcal{N}_t'(p)|r| - 2\theta(p-r)\mathcal{N}_t(p-r)], \tag{23}$$

where $G_0=8\pi^2e^2|U^0|^2(1+\xi^2)\rho_{0t}\rho_0\Delta_0/h$, $\rho_G=\rho_0|r-p|$, $\rho_t(r)=\rho_{0t}\mathcal{N}_t(r)$, $\mathcal{N}_t(x)=|x|/\sqrt{x^2-1}\,\theta(|x|-1)$, $\mathrm{sgn}(x)$ denotes the signum function, $\rho_0=6\sqrt{3}/(2\pi\hbar^2v_F^2)$ (Ref. 1) and ρ_{0t} is the constant DOS of the metallic tip. For graphene with $E_F=r=0$, $dG/dV\sim\mathrm{sgn}(V)\mathcal{N}_t(-V)$, i.e., the tip DOS is given by the derivative of the tunneling conductance. For large E_F away from the Dirac point, the first term of G becomes large and reflects the tip DOS. In between these extremes, when $E_F\sim eV$, neither G nor dG/dV reflects the DOS. In this region, the signature of the Dirac point appears through a cusp (discontinuity) in $G(dG/dV)$ at $eV=-E_F-\Delta_0$ arising from the contribution of the second (third) term in Eq. (22) [Eq. (23)]. These features, shown in Fig. 2, distinguish such graphene STM spectra with their conventional counterparts.[15]

Next, we turn to the case of impurity-doped graphene and consider a metallic tip with constant DOS. The contribution to the tunneling conductance from the impurity (after subtracting the graphene background) at $T=0$ [Eq. (21)] is

$$G_{\mathrm{imp}} = G_0'\frac{|B(V)|^2}{\mathrm{Im}\,\Sigma_d(V)}\frac{|q(V)|^2-1+2\,\mathrm{Re}[q(V)]\chi(V)}{\Lambda[1+\chi^2(V)]}, \tag{24}$$

where $G_0'=2e^2\rho_{0t}\Lambda/h$. Such tunneling conductances are known to have peak/antiresonance/dip feature at zero bias for $|q|\gg1/\simeq1/\ll1$.[13] In conventional metals or earlier STM studies in graphene,[10] U^0 has been taken to be a fixed parameter independent of the position of the impurity. However, as we show here, the situation in graphene necessitates a closer attention. To this end, we note that U^0 is proportional to the probability amplitude of the Dirac quasiparticles in graphene to hop to the tip and its strength can be estimated using the well-known Bardeen tunneling formula:[18] $U^0\sim\int d^2r[\phi_\nu^\dagger(z)\partial_z\Psi_G(\vec{r},z)-\Psi_G^\dagger(\vec{r},z)\partial_z\phi_\nu(z)]\sim\Psi_G(\vec{r}_0,z_0)$, where the last similarity is obtained by a careful evaluation of the surface integral $\int d^2r$ over a surface between the graphene and the tip parallel to the graphene sheet,[19] $(\vec{r}_0,z_0)$ is the coordinate of the tip center, $\phi_\nu(z)$ is tip electron wave function, and the wave function of the graphene electrons $\Psi_G(\vec{r},z)$ around $K(K')$ valley, can be written, within tight-binding approximation, as[20]

$$\Psi_G(\vec{r},z) = \frac{1}{\sqrt{N}}\sum_{R_i^A} e^{i[\{\vec{K}(\vec{K}')+\vec{\delta k}\}\cdot\vec{R}_i^A]}[\varphi(\vec{r}-\vec{R}_i^A) + e^{+(-)i\theta_k}\varphi(\vec{r}-\vec{R}_i^B)]f(z). \tag{25}$$

Here $\theta_k=\arctan(k_y/k_x)$, $\vec{\delta k}$ is the Fermi wave vector as measured from the Dirac points with $|\vec{\delta k}|\ll|\vec{K}(\vec{K}')|$ for all E_F, $\varphi(\vec{r})$ are localized p_z orbital wave functions, N is a normalization constant, $f(z)$ is a decaying function of z with decay length set by work function of graphene, and $R_i^{A(B)}=n\hat{a}_1+m\hat{a}_2(\hat{a}_2-\hat{y})$ with integers n and m denote coordinates of the graphene lattice sites (Fig. 1).[20] When the impurity and the STM tip is atop the center of the hexagon, pseudospin symmetry necessitates $\varphi(\vec{r}_0-\vec{R}_i^{A,B})$ to be identical for all neighboring A and B sublattice points 1–6 surrounding the impurity (Fig. 1). Consequently, the sum over lattice vectors R_i^A in Eq. (25) reduces to a sum over the phase factors $\exp(i[\{\vec{K}(\vec{K}')+\vec{\delta k}\}\cdot\vec{R}_i^A])$ for these lattice points. It is easy to check that this sum vanishes for both Dirac points (when $|\vec{\delta k}|=0$). Thus the only contribution to $\Psi_G(\vec{r}_0,z_0)$ comes from the second and further neighbor sites for which the amplitude of localized wave functions $\varphi(\vec{r}_0-\vec{R}_i^{A/B})$ are small. For finite E_F, $(\vec{\delta k}\neq0)$ there is a finite but small contribution $[\mathrm{O}(|\vec{\delta k}|/|\vec{K}|)]$ to $\Psi_G(\vec{r}_0,z_0)$ from the nearest-neighbor sites. Thus $\Psi_G(\vec{r}_0,z_0)$ and hence U^0 is drastically reduced when the impurity is atop the hexagon center. In this case, we expect $U^0\ll W^0$ and hence $|q|\gg1$ [Eq. (20)] leading to a peaked spectra for all E_F. In contrast, for the impurity atom atop a site, there is no such symmetry induced cancellation and $\psi_G(\vec{r}_0,z_0)$ receives maximal contribution from the nearest graphene site directly below the tip. Thus we expect $|U^0|\gg|W^0|$ (since it is easier for the tip electrons to tunnel to

delocalized graphene band than to a localized impurity level) leading to $q \simeq I_1/I_2 \simeq -\ln|1-\Lambda^2/(eV+E_F)^2|/\pi$. For large $|eV+E_F|$ and impurity atop a site, $q \leq 1$ leading to a dip or an antiresonance in $G_{\rm imp}$ which is qualitatively distinct from the peaked spectra for impurity atop the hexagon center. As $E_F \to 0$, q diverges logarithmically for small eV. However, it can be shown that in this regime χ shows a stronger linear divergence for $eV \neq \epsilon_d$ which suppresses $G_{\rm imp}$. At $eV=\epsilon_d$, the divergence of χ also becomes logarithmic and we expect a peak of $G_{\rm imp}$. Note that these effects are independent of Σ_d and hence of the precise nature of the impurity. Such an impurity position-dependent peak/dip structure of $G_{\rm imp}$ has been observed for magnetic impurities in Ref. 9 for $E_F \gg eV$.

To demonstrate this feature, we restrict ourselves to impurities with small Hubbard U and compute the self-energy of the impurity electrons within a mean-field theory where $Un_\sigma n_{\bar\sigma} = U\langle n_\sigma\rangle n_{\bar\sigma}$ leading to spin-dependent on-site impurity energy $\epsilon_\sigma = \epsilon_d + U\langle n_{\bar\sigma}\rangle$.[7] Using Eqs. (1) and (5), one then obtains the mean-field advanced impurity Green's function $\mathcal{G}^{\rm imp}_\sigma(\omega) = [\omega - \epsilon_\sigma - \Sigma_d(\omega)]^{-1}$ where the impurity self-energy is given by $\Sigma_d(\omega) = |V^0|^2(I_1 + iI_2)$ and mean-field self-consistency condition demands $n_\sigma = \int d\omega/\pi\ {\rm Im}\ \mathcal{G}^{\rm imp}_\sigma(\omega)$. Following Ref. 7, we solve these equations to get $\chi(\epsilon)$, and Im $\Sigma_d(\epsilon)$ which can be substituted in Eq. (24) to obtain $G_{\rm imp}$. We note, from Eqs. (20) and (24), that $G_{\rm imp}/G_0'$ depends on the ratios E_F/Λ, V^0/Λ, and W^0/U^0 which cannot be quantitatively determined from the Dirac-Anderson model. We therefore treat them as parameters of the theory[1,7] and compute $G_{\rm imp}$ for their representative values as shown in Fig. 3. In accordance with earlier discussions, we find that for large $E_F/\Lambda = 0.3$, $G_{\rm imp}$ has qualitatively different features; for the impurity at the center of the hexagon, it shows a peak (left panel) while for that atop a site (right panel), it shows a dip. The change in $G_{\rm imp}$ from a dip to a peak via an antiresonance as a function of E_F/Λ when the impurity is atop a site can be seen from right panel of Fig. 3. In contrast, the left panel always shows peak spectra.

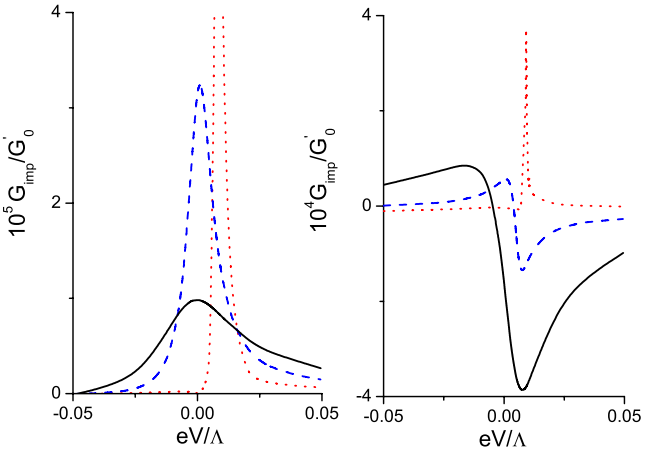

FIG. 3. (Color online) Plot of $G_{\rm imp}$ as a function of V for $|W^0/U^0| = 0.05$ (right; impurity atop a site) and 2 (left; impurity atop hexagon center) for $E_F/\Lambda = 0.3$, 0.1, and 0 (black solid, blue dashed, and red dotted lines, respectively). Plot parameters are $5U = V^0 = 0.05\Lambda$, $W^0 = 0.0005\Lambda$, and $\epsilon_d = 0$.

IV. CONCLUSION

In conclusion, we have shown that the tunneling conductance spectra of both doped and undoped graphene have unconventional features not discussed in earlier studies.[10] In particular, the STM spectra of doped graphene depend qualitatively on the position of the impurity in the graphene matrix. This feature is demonstrated to be a direct consequence of pseudopsin symmetry and Dirac nature of graphene quasiparticles.

Further experimental verification of our work would involve measuring tunneling conductance of doped and undoped graphene by varying E_F. For undoped graphene with $E_F = 0$, we propose to measure the tunneling conductance spectra using a superconducting tip and verify that $dG/dV \sim \rho_t\ {\rm sgn}(V)$. For small $E_F > 0$, where it is possible to access the regime $eV > E_F$ in experiments, we predict a cusp (discontinuity) in $G(dG/dV)$ at $eV = -E_F - \Delta_0$ as a signature of the Dirac point. The variation in the shape of the spectra of impurity-doped graphene with impurity atop a site may also be experimentally studied.

We also note that the theory of tunneling conductance derived here should also be applicable to the impurity-doped Dirac electrons on the surface of strong topological insulators with a single Dirac cone.[21] In this case, we expect to find that the STM spectra should change from a dip to a peak through an antiresonance as the Fermi energy is tuned toward the Dirac point. This behavior is qualitatively similar to that shown in the right panel of Fig. 3. However, such a controlled tuning of Fermi energy of topological insulators seems to be experimentally more difficult than graphene.

Note added. Recently, we came to know of Ref. 22 with related results.

ACKNOWLEDGMENTS

K.S. thanks A. Castro Neto, V. N. Kotov, and H. Manoharan for discussions.

[1] A. H. Castro Neto, F. Guinea, N. M. R. Peres, K. S. Novoselov, and A. K. Geim, Rev. Mod. Phys. **81**, 109 (2009); T. Ando, J. Phys. Soc. Jpn. **74**, 777 (2005).

[2] V. P. Gusynin and S. G. Sharapov, Phys. Rev. Lett. **95**, 146801 (2005); N. M. R. Peres, F. Guinea, and A. H. Castro Neto, Phys. Rev. B **73**, 125411 (2006); V. Lukose, R. Shankar, and G. Baskaran, Phys. Rev. Lett. **98**, 116802 (2007).

[3] K. S. Novoselov, A. K. Geim, S. V. Morozov, D. Jiang, M. I. Katsnelson, I. V. Grigorieva, S. V. Dubonos, and A. A. Firsov, Nature (London) **438**, 197 (2005); Y. Zhang, Y.-W. Tan, H. L. Stormer, and P. Kim, *ibid.* **438**, 201 (2005); K. S. Novoselov, E. McCann, S. V. Morozov, V. I. Falko, M. I. Katsnelson, U.

Zeitler, D. Jiang, F. Schedin, and A. K. Geim, Nat. Phys. **2**, 177 (2006).
[4] C. W. J. Beenakker, Phys. Rev. Lett. **97**, 067007 (2006); M. Titov and C. W. J Beenakker, Phys. Rev. B **74**, 041401(R) (2006).
[5] S. Bhattacharjee and K. Sengupta, Phys. Rev. Lett. **97**, 217001 (2006); S. Bhattacharjee, M. Maiti, and K. Sengupta, Phys. Rev. B **76**, 184514 (2007); M. Maiti and K. Sengupta, *ibid.* **76**, 054513 (2007).
[6] K. Sengupta and G. Baskaran, Phys. Rev. B **77**, 045417 (2008); M. Hentschel and F. Guinea, *ibid.* **76**, 115407 (2007).
[7] B. Uchoa, V. N. Kotov, N. M. R. Peres, and A. H. Castro Neto, Phys. Rev. Lett. **101**, 026805 (2008).
[8] F. Schedin, A. K. Geim, S. V. Morozov, E. W. Hill, P. Blake, M. I. Katsnelson, and K. S. Novoselov, Nature Mater. **6**, 652 (2007).
[9] H. Manoharan (private communication).
[10] N. M. R. Peres, S.-W. Tsai, J. E. Santos, and R. M. Ribeiro, Phys. Rev. B **79**, 155442 (2009); H. Zhuang, Q. Shun, and X. C. Xie, EPL **86**, 58004 (2009); P. S. Cornaglia, G. Usaj, and C. A. Balseiro, Phys. Rev. Lett. **102**, 046801 (2009); N. M. R. Peres, L. Yang, and S.-W. Tsai, New J. Phys. **11**, 095007 (2009); O. Poplavskyy, M. O. Goerbig, and C. Morais Smith, Phys. Rev. B **80**, 195414 (2009).
[11] I. Brihuega, P. Mallet, C. Bena, S. Bose, C. Michaelis, L. Vitali, F. Varchon, L. Magaud, K. Kern, and J. Y. Veuillen, Phys. Rev. Lett. **101**, 206802 (2008).
[12] T. Valla, A. V. Fedorov, Jinho Lee, J. C. Davis, and G. D. Gu, Science **314**, 1914 (2006); see, e.g., O. Fischer, M. Kugler, I. Maggio-Aprile, C. Berthod, and C. Renner, Rev. Mod. Phys. **79**, 353 (2007).
[13] U. Fano, Phys. Rev. **124**, 1866 (1961); V. Madhavan, W. Chen, T. Jamneala, M. F. Crommie, and N. S. Wingreen, Science **280**, 567 (1998).
[14] Y. Meir and N. S. Wingreen, Phys. Rev. Lett. **68**, 2512 (1992); Y. Meir, N. S. Wingreen, and P. A. Lee, *ibid.* **70**, 2601 (1993).
[15] S. H. Pan, E. W. Hudson, and J. C. Davis, Appl. Phys. Lett. **73**, 2992 (1998); A. Kohen, Th. Proslier, T. Cren, Y. Noat, W. Sacks, H. Berger, and D. Roditchev, Phys. Rev. Lett. **97**, 027001 (2006); I. Guillamon, H. Suderow, S. Vieira, and P. Rodiere, Physica C **468**, 537 (2008).
[16] P. W. Anderson, Phys. Rev. **124**, 41 (1961).
[17] See, for example, G. D. Mahan, *Many-Particle Physics* (Plenum Press, New York, 1981).
[18] J. Bardeen, Phys. Rev. Lett. **6**, 57 (1961).
[19] J. Tersoff and D. R. Hamann, Phys. Rev. Lett. **50**, 1998 (1983).
[20] C. Bena and G. Montambaux, New J. Phys. **11**, 095003 (2009).
[21] D. Hsieh, D. Qian, L. Wray, Y. Xia, Y. S. Hor, R. J. Cava, and M. Z. Hasan, Nature (London) **452**, 970 (2008); Y. Xia, D. Qian, D. Hsieh, L. Wray, A. Pal, H. Lin, A. Bansil, D. Grauer, Y. S. Hor, R. J. Cava, and M. Z. Hasan, Nat. Phys. **5**, 398 (2009).
[22] B. Uchoa, L. Yang, S.-W. Tsai, N. M. R. Peres, and A. H. Castro Neto, Phys. Rev. Lett. **103**, 206804 (2009).